nature geoscience

ARTICLES

https://doi.org/10.1038/s41561-020-0557-6

The river–groundwater interface as a hotspot for arsenic release

Ilka Wallis[1,2]✉, Henning Prommer[2,3,4], Michael Berg[5], Adam J. Siade[2,3,4], Jing Sun[3,4,8] and Rolf Kipfer[5,6,7]

Geogenic groundwater arsenic (As) contamination is pervasive in many aquifers in south and southeast Asia. It is feared that recent increases in groundwater abstractions could induce the migration of high-As groundwaters into previously As-safe aquifers. Here we study an As-contaminated aquifer in Van Phuc, Vietnam, located ~10 km southeast of Hanoi on the banks of the Red River, which is affected by large-scale groundwater abstraction. We used numerical model simulations to integrate the groundwater flow and biogeochemical reaction processes at the aquifer scale, constrained by detailed hydraulic, environmental tracer, hydrochemical and mineralogical data. Our simulations provide a mechanistic reconstruction of the anthropogenically induced spatiotemporal variations in groundwater flow and biogeochemical dynamics and determine the evolution of the migration rate and mass balance of As over several decades. We found that the riverbed–aquifer interface constitutes a biogeochemical reaction hotspot that acts as the main source of elevated As concentrations. We show that a sustained As release relies on regular replenishment of river muds rich in labile organic matter and reactive iron oxides and that pumping-induced groundwater flow may facilitate As migration over distances of several kilometres into adjacent aquifers.

Geogenic groundwater arsenic (As) contamination is a problem of global significance, with noteworthy occurrences in large parts of the alluvial and deltaic aquifers in south and southeast Asia[1,2]. Most regional reconnaissance studies show a relation of groundwater As concentrations with depth[1] and sediment age[3]. Deeper (>50 m) and therefore commonly 'older' aquifers show significantly lower dissolved As concentrations, whereas groundwaters in contact with shallower (<50 m), commonly 'younger' (Holocene) sediments often exceed the World Health Organisation guideline value of 10 μg l^{-1}, sometimes by a factor of 100. Consequently, targeting low-As aquifers has become the key mitigation strategy to reduce human As exposure. However, fears have emerged that As-rich groundwater from overlying aquifers could be drawn into currently unaffected aquifers[2,4–9].

The presence of As in Holocene groundwaters is generally assumed to originate from the recent As-bearing deposition of sediments that have been transported downstream by rivers that drain orogenies such as the Himalayas[1,10]. Microbially driven reductive dissolution of Fe(III) oxides by natural organic carbon is assumed to be the primary mechanism for the release of As from these deposited alluvial river flood plain and delta sediments. Although there is strong evidence that the relative abundance and reactivity of Fe(III) oxides and organic carbon plays a key role in controlling As release[11], the mechanistic understanding of As distribution patterns within the groundwater remains fragmented and poorly constrained[1,7]. This includes uncertainty about the relative importance of different organic matter (OM) sources[1], such as buried sediment-bound organic matter (SOM)[12,13], dissolved organic carbon (DOC) inputs to aquifers via wetlands[14–16], irrigation and its associated recharge of DOC, as well as buried peat layers[12,17]. Furthermore, groundwater As concentrations seldom follow continuous gradients but often show steep variations over small distances with no apparent systematic relationship between the solid-phase and dissolved As concentrations[4,12,18–20]. Clearly, As partitioning between the solid and dissolved phases could also be influenced by groundwater flow processes that may impact the evolution of As concentration patterns more strongly than chemical or microbial processes. These and other knowledge gaps hinder the development of a mechanistic understanding of the local-scale controls on As liberation and migration; however, this can potentially be remedied with a holistic exploration of key hydro(bio)geochemical processes through numerical modelling. In this study, we integrate detailed field observations (Extended Data Tables 2 and 3) from a large number of earlier studies[2,4,7,10,21–23] to guide the development and test the plausibility of conceptual and numerical models of As mobilization and transport, which in turn exemplify the primary controls of As plume formation.

Large-scale groundwater abstraction induces river-water intrusion

For more than 50 years, Hanoi's increasing groundwater demand has fundamentally changed the regional groundwater flow system[2,7]. Under undisturbed conditions, recharge of the Holocene aquifers occurred mainly through the low-permeability clay and silty overburden at relatively low rates[14], and net annual groundwater flow was directed towards the Red River. However, induced by successively increasing abstraction, hydraulic gradients at the study site have reversed and transformed the Red River locally from a net-gaining to a net-losing river[7]. Groundwater flow at Van Phuc is now consistently directed in a northwest direction towards the cone of depression beneath Hanoi[4,7,10] (Fig. 1).

[1]College of Science and Engineering, Flinders University, Adelaide, South Australia, Australia. [2]National Centre for Groundwater Research and Training, Flinders University, Adelaide, South Australia, Australia. [3]School of Earth Sciences, The University of Western Australia, Crawley, Western Australia, Australia. [4]CSIRO Land and Water, Wembley, Western Australia, Australia. [5]Eawag, Swiss Federal Institute of Aquatic Science and Technology, Dübendorf, Switzerland. [6]Institute of Biogeochemistry and Pollutant Dynamics, ETH Zurich, Zurich, Switzerland. [7]Institute of Geochemistry and Petrology, ETH Zurich, Zurich, Switzerland. [8]Present address: State Key Laboratory of Environmental Geochemistry, Institute of Geochemistry, Chinese Academy of Sciences, Guiyang, China. ✉e-mail: ilka.wallis@flinders.edu.au

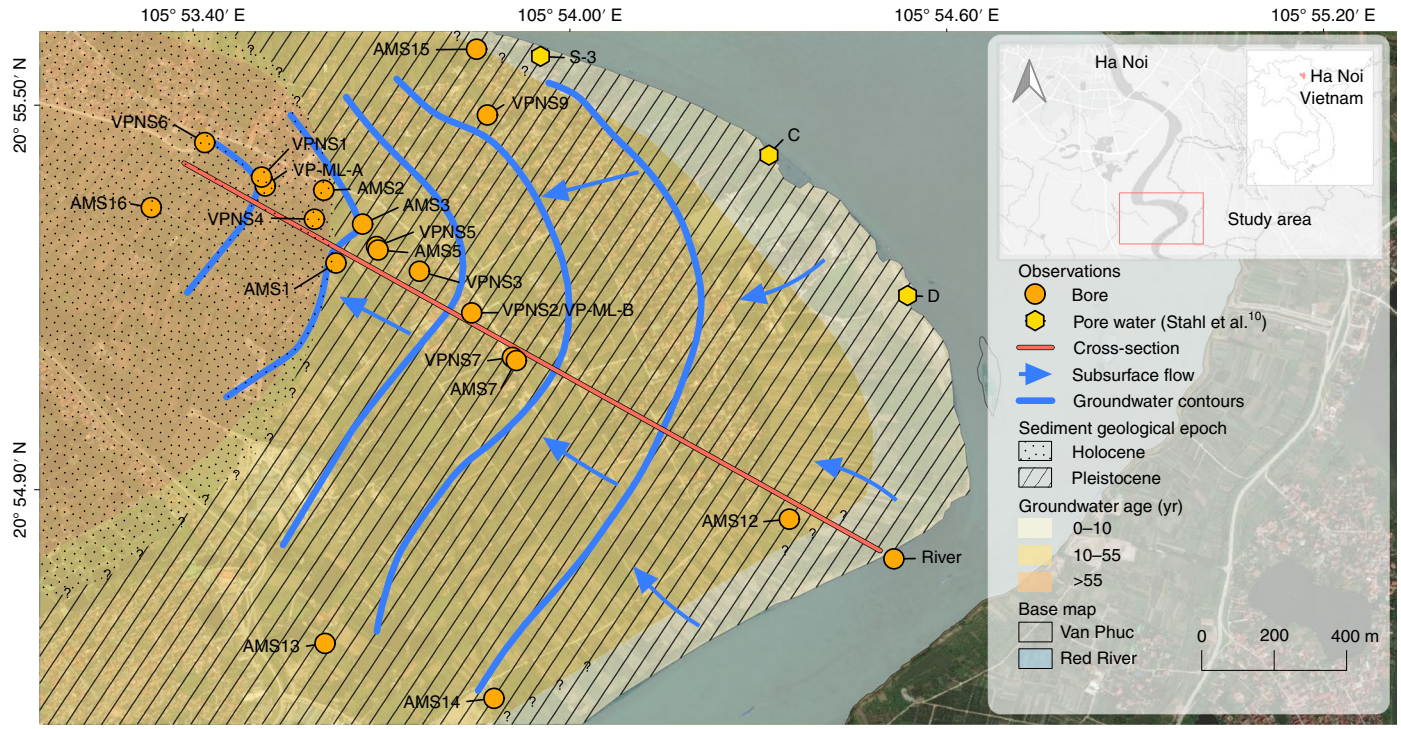

Fig. 1 | Field site, observation bores and approximate groundwater flow field in the study area. Water level contours assessed on the basis of hydraulic heads (head data from November 2006 and June 2010) and main groundwater flow direction; groundwater ages are inferred from ^{3}H and $^{3}He_{tri}$ concentration data. Orange line, location of modelled cross-section. Approximate distribution of Holocene and Pleistocene sediments reproduced from van Geen et al.[7]. Base map credits: Esri, DigitalGlobe, GeoEye, i-cubed, USDA FSA, USGS, AEX, Getmapping, Aerogrid, IGN, IGP, swisstopo, the GIS User Community, DeLorme, HERE and MapmyIndia.

Based on the available hydrogeological, hydraulic, tritium (^{3}H) and tritiogenic helium ($^{3}He_{tri}$) data, we used transient two-dimensional (2D) numerical simulations of groundwater flow and solute transport to reconstruct the site's groundwater dynamics over a 60-year period. Originating at the river bank and aligned along the main groundwater flow direction, the model successfully mimics the temporally and spatially varying groundwater flow field between the approximate start of the flow reversal (~1950) and today (Figs. 1–3). The results show that groundwater in the Holocene aquifer is generally of a short residence time, which ranges from 0 to ~45 years, except for waters at a greater depth (>40 m (Figs. 4 and 5)). In contrast, the groundwater in the zone occupied by Pleistocene sediments contains neither ^{3}H nor $^{3}He_{tri}$, which implies that the water infiltrated before nuclear bomb testing, that is, >55 years ago (Figs. 1 and 3). In agreement with van Geen et al.[7] the ^{3}H- and $^{3}He_{tri}$-constrained simulations suggest that groundwater flow velocities in the Holocene aquifer increased from <1 m yr^{-1} in 1950 to the current average of 40 m yr^{-1}.

River-mud deposits as biogeochemical reaction hotspots

Building on the groundwater flow simulations, multiple plausible conceptual and numerical model variants for the site's reactive transport processes were investigated (CM1–CM6, Figs. 2, 4 and 5 and Extended Data Table 1). Variant CM6 includes the most comprehensive range of biogeochemical reactions and the entire range of potential organic carbon sources within the investigated system. This scenario served as the basis for an inversion process, which included the joint calibration of flow, solute and reactive transport parameters, followed by a linearized uncertainty assessment for all the model parameters (Methods and Supplementary Tables 5 and 6). This procedure revealed independently which processes most probably contributed to the field-observed flow and geochemical patterns and isolated the most plausible conceptual model. This verifiable procedure resulted in a firm mechanistic understanding of today's observed groundwater As distribution pattern within the Holocene aquifer and its evolution over the past 60 years (Figs. 3–5).

The core of the biogeochemical reaction network that was found to best describe the observations encompasses (1) OM mineralization under aerobic, denitrifying, sulfate-reducing and Fe-reducing conditions, (2) precipitation as well as reductive dissolution of Fe(III) oxides, (3) calcite dissolution and precipitation and (4) surface complexation reactions of As with Fe(III) oxides. Process (4) is not only important to explain As release and immobilization, but also the time-varying spatial distribution of the sorbed and dissolved As mass within the aquifer. The inversion process revealed further that organic carbon sources had a clearly different reactivity depending on their lithological association. SOM reactivity in the Holocene sands was revealed to be negligible, whereas reactivities were distinctively higher in the clay/silt deposits (~0.06 mM C yr^{-1}) and higher again by a factor of ~30 in the river muds.

Plotting the dissolved concentrations of key reactive species as a function of groundwater residence time calculated from ^{3}H and $^{3}He_{tri}$ concentrations (Fig. 4) and as a function of distance from the river (Supplementary Fig. 7) summarizes the trends of the simulated and observed hydrochemical changes. It is evident that the steepest concentration gradients occur in proximity to the river bank, that is, within the recently recharged groundwaters. Here, the dissolved oxidants O_2, NO_3^- and SO_4^{2-} that are contained in the intruding Red River water, together with Fe(III) oxides, are consumed rapidly alongside significant increases in the concentrations of Ca, HCO_3^-, As_{tot}, Fe^{2+}, NH_4^+ and P. Besides the concentration changes that are directly associated with the primary redox reactions, calcite and silica dissolution also proceed such that, overall, the electrical conductivity (EC) rapidly increases from ~300 µS cm^{-1}

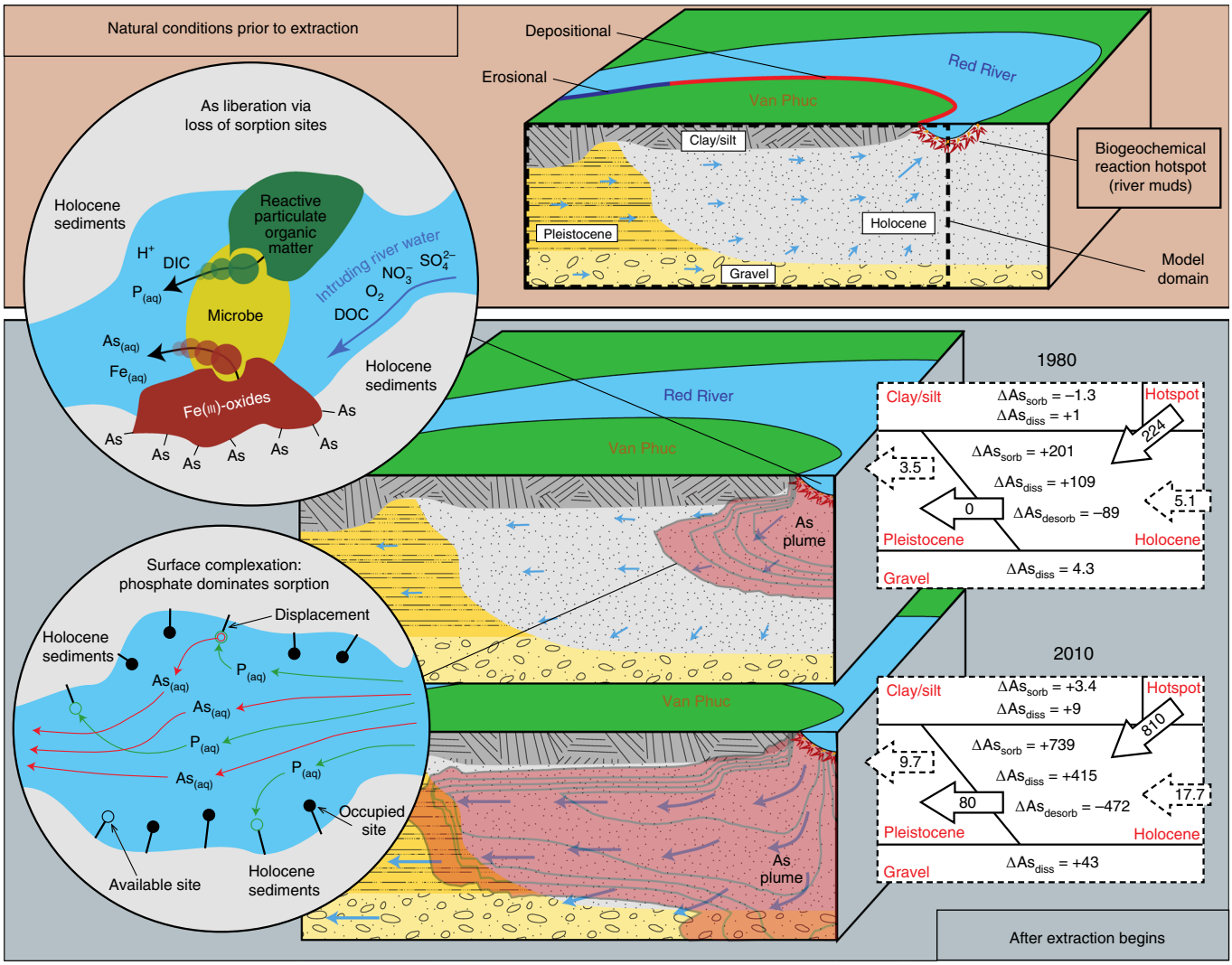

Fig. 2 | Conceptual model of As plume evolution at Van Phuc. Successive increases in groundwater abstraction since the 1950s have induced a reversal of the natural groundwater flow direction and the influx of riverine water into the Holocene aquifer and given rise to a hotspot for As release. Sustained As release from the hotspot relies on a continuous co-deposition of labile organic carbon and As-hosting reactive Fe oxides in depositional zones along the Red River. Advective fluxes draw the As-enriched pore water at the river–groundwater interface into the aquifer where an As plume is formed. The influx and outflux of As from river muds and over aquifer boundaries are displayed for two time intervals as well as the resulting change in released (As_{diss}), adsorbed (As_{sorb}) and desorbed As mass (As_{desorb}) for the Holocene sands, the gravel deposits and the clay/silt overburden. Further details are given in the Supplementary Information.

(river) to >1,000 µS cm^{-1} in the groundwater. Thereafter, data scatter around the resultant elevated concentrations mark groundwater of longer residence time that infiltrated the Holocene aquifer between 10 and 50 years ago (Fig. 4). Superimposed on this trend are local concentration variations induced by the mineralization of OM hosted in the silt/clay deposits capping the Holocene sands and the diffusional influx of affected solutes (for example, HCO_3^- and Fe_{tot} (Fig. 4)).

The observed and simulated steep concentration gradients in proximity to the river bank strongly suggest that the river-mud deposits act as a biogeochemical reaction hotspot (BRH) in which the regular deposition not only of As-containing Fe(III) oxides but also of highly reactive organic carbon plays a key role. Induced by the rapid OM degradation, reductive dissolution of Fe(III) oxides leads to a successive loss of sorption sites, which fuels a sustained As release at and near the river–groundwater interface to form the As plume that is now observed in the aquifer. In contrast, slow infiltration of organic-rich water through the overlain clay and silt deposits constitutes a relatively minor contribution to As release (Fig. 2 and Supplementary Table 4). Although these clay and silt deposits contain elevated concentrations of OM (0.01–0.82 wt% at 0–25 metres below ground level[23]) and pore water with elevated concentrations of As_{tot}, Fe^{2+}, NH_4^+, HCO_3^- and P, consistent with those of many As source zones, the water flux from these low-permeability deposits is too low to provide a significant impact on the overall As mass flux in the Holocene aquifer (<5%).

Finally, our modelling results suggest that the SOM that prevails in the Holocene aquifer (Supplementary Table 4) contributes only minimally to the As mass budget. If an elevated SOM reactivity in the Holocene aquifer was assumed (model variant CM5), the steep concentration gradients near the river–aquifer interface could not be reproduced. Instead, a steady and continuous increase in concentrations occurred along the flow path (Fig. 4e). Therefore, in situ As release by Fe(III) oxide reduction plays a minor role in the formation of the As plume compared to the contribution from As release at the river–groundwater interface. This finding is consistent with

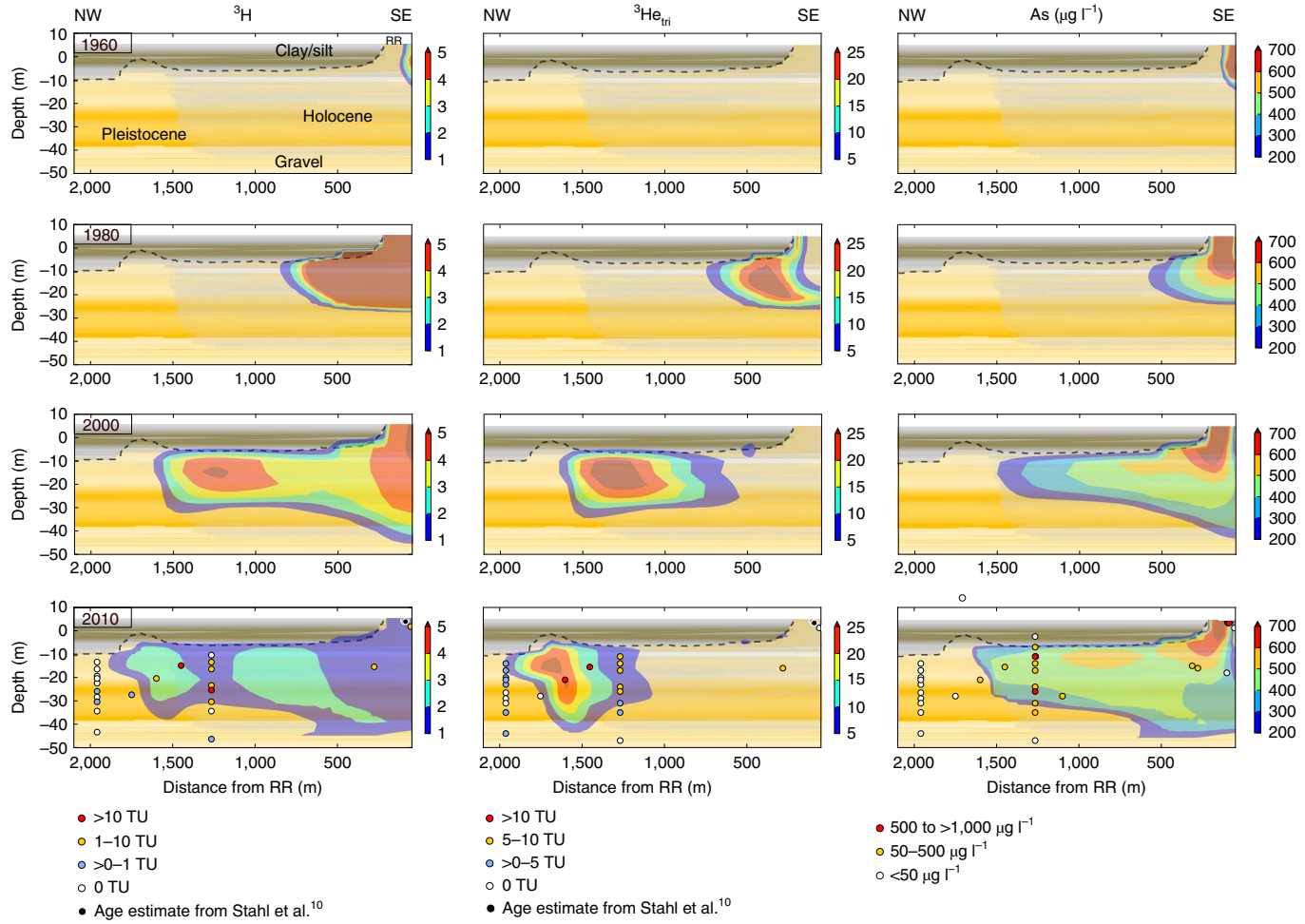

Fig. 3 | Simulated concentrations of ^{3}H, ^{3}He$_{tri}$ and As$_{tot}$ (1960–2010) along the cross-section from the Red River (RR) towards the northwest. Observations (Fig. 1) are shown by the coloured dots along with the observed concentrations. The approximate boundary between the confining clay/silt layer and sand and gravel deposits of Holocene and Pleistocene age is shown by the dashed line. Simulations of groundwater flow and solute transport, constrained by hydraulic, ^{3}H and ^{3}He$_{tri}$ measurements, reconstruct the groundwater dynamics over a 60-yr period between the approximate start of pumping-induced flow reversal (~1950) and today. Groundwaters in the Holocene aquifer are generally 'young', (0 to ~45 yr), whereas groundwaters in Pleistocene sediments contain broadly no ^{3}H or ^{3}He$_{tri}$, which suggests that water infiltrated before the atmospheric bomb tests (that is, >55 years ago). The currently observed pattern of dissolved As can be linked to the successively increasing river-water intrusion in response to Hanoi's growing water demand. NW, northwest; SE, southeast; TU, tritium units. Colour scale bars are TU units for tritium and helium, and μg l^{-1} for As$_{tot}$.

the unvaryingly low SOM concentrations found in the Holocene aquifer (<0.03 wt% (Supplementary Fig. 1)).

Identifying the river–groundwater interface as a BHR is corroborated by earlier observations in the region, which include laboratory incubation experiments that documented extensive As release from saturated near-surface sediments of the Mekong Delta but little As release from deeper aquifer sediments[16]. The reactivity of native SOM was found to be insufficient to fuel a significant reductive dissolution of the native Fe(III) oxides in the deeper clays and aquifer sands. In situ As release measurements within river muds along the Red River[10] and incubation experiments with Red River sediments from other sites[24] also support our finding.

As plume dynamics

Emerging from the As release hotspot at the riverbed, water enriched in As successively displaced the ambient groundwater that prevailed in the fluviatile sediments prior to 1950. The most plausible conceptual/numerical model (CM6), which produced the closest match to observed concentration patterns (Supplementary Table 5), suggests that the currently observed spatial distribution of groundwater As can be linked to the successively increasing rates of river-water intrusion. Starting with the intrusion of river water into the Holocene aquifer, dissolved As concentrations at the river–groundwater interface increased to >500 μg l^{-1} (Figs. 3–5). The simulations illustrate that the front of the As plume migrated >1,700 m over the past 60 years, from the river–groundwater interface to its current position.

The ratio of the rates of river-water infiltration and net As release from the hotspot in combination with the adsorption affinity of the Fe oxides in the Holocene sands thereby govern the total As plume mass and its front propagation with time. As release rates from the river muds remain below our model-estimated As replenishment rate of 0.003 μM As day^{-1} until ~20 years after the commencement of pumping in Hanoi (Supplementary Fig. 11). In the subsequent years, however, with advective velocities that exceed 8.8 m yr^{-1}, As release started to surpass As replenishment, which subsequently resulted in a slow depletion of the river-mud As pool. At the end of the simulation period, the net As release rate increased to ~0.017 μM As day^{-1}, with the overall As pool diminishing to ~60% of its initial mass. The decreasing As pool will ultimately lead to an increased dilution of the released As and decreasing dissolved As concentrations within the Holocene aquifer, as observed for a study site in Nam Du, east of Hanoi[25]. Our modelling results infer

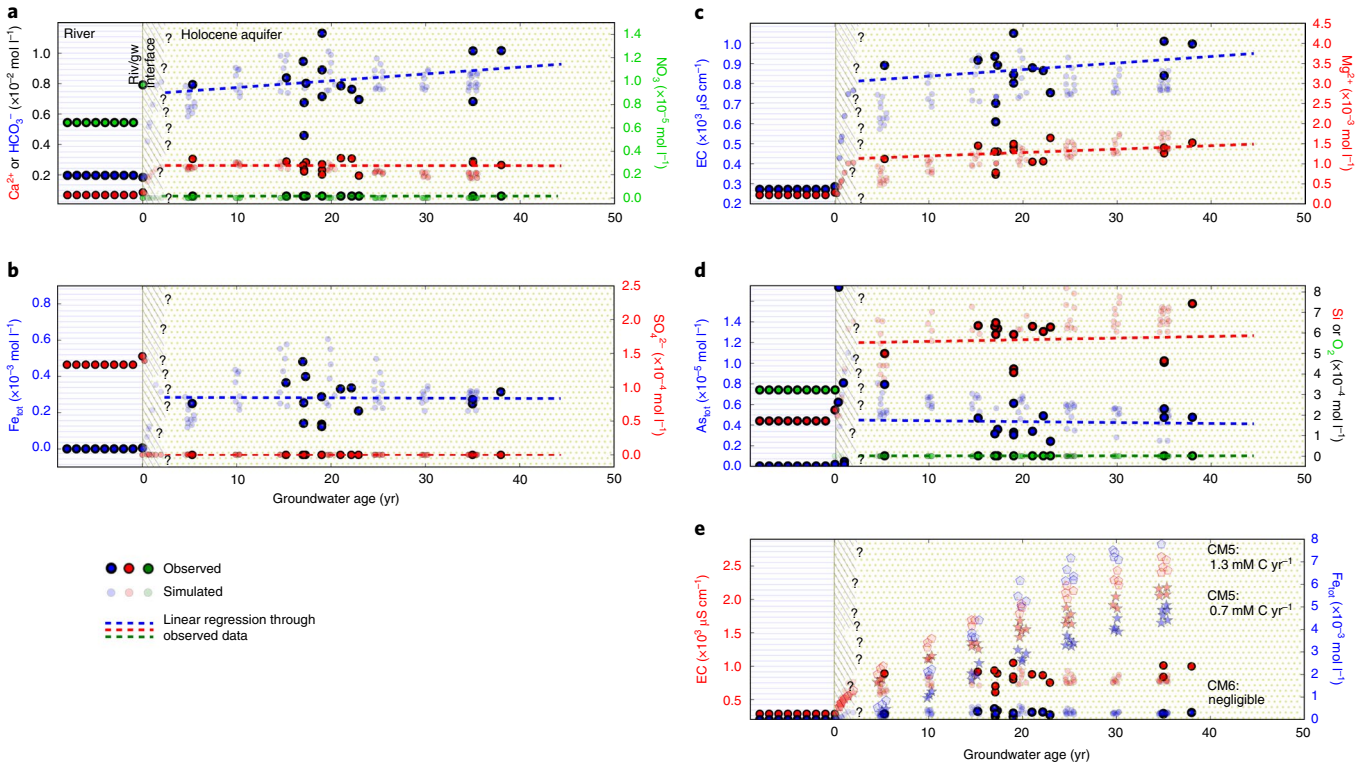

Fig. 4 | Observed and simulated concentrations and ECs versus apparent groundwater age. a–d, Observed (Stahl et al.[10] and Supplementary Tables 1 and 2) and simulated (CM6 model variant) concentrations and EC versus apparent $^3H/^3He_{tri}$ ages from river water to Holocene groundwater. **e**, EC and Fe_{tot} under varying OM degradation rates within the Holocene sands (CM5 and CM6). Simulated concentrations (faint dots) are shown for all the model cells with $^3H/^3He_{tri}$ ages of 5, 10, 15, 20, 25, 30 and 35 yr within the depth range 17–45 m, consistent with the depth range of the observation bores, which results in a point cloud of simulated concentrations for each groundwater age group. Simulated concentrations in the river muds are based on model cells with $^3H/^3He_{tri}$ ages <2 yr.

that river-mud replenishment is required to allow for a sustained As release over the entire simulation period.

In addition to As release from river muds, in situ release of As also emerged within the Holocene sands as a consequence of river-water intrusion. Interestingly, this release, although predominantly linked to the displacement of As from Fe-hosted sorption sites, occurs in the absence of excessive reductive dissolution of Fe oxides. The differing hydrochemical characteristics of the intruding river water, in particular the elevated phosphate concentrations that originate from OM mineralization at the groundwater–river interface, reduce the affinity for As sorption. This decreased affinity causes the aqueous As plume mass to increase and spread at a faster rate than if the reductive dissolution of Fe oxides was the sole source of As. Simultaneously, but spatially apart, released As is partially resorbed downgradient of the plume front (Supplementary Figs. 8 and 9). Although As in situ release initially provided a negligible contribution to the overall As plume mass, its overall contribution increased over time to ~35% (Fig. 2 and Supplementary Table 4) as the infiltrating river water occupied steadily increasing volumes of the Holocene aquifer, with the remainder originating from river muds. The modelling results suggest an average As release of 0.1 µM yr^{-1}, which compares well with experimentally determined rates of 0.02–0.35 µM yr^{-1} for Holocene sediments north of Hanoi[3] and 0.18 µM yr^{-1} for a site northwest of Hanoi[26] (Supplementary Fig. 12).

Physicochemical controls of As release rates

Despite the increase in river-water intrusion over the past ~60 years, the OM degradation rate in the river muds remained approximately constant (1.9 mM C yr^{-1} (Supplementary Fig. 11)) due to sustained Fe reduction. The simulated average net As release rate within the river muds is in the range of 6 µM yr^{-1}. This model-estimated rate is in good agreement with the experimentally determined rate of Stahl et al.[10], who measured net As release rates at the river–aquifer interface that ranged between <0.15 and 55 µM yr^{-1}, and laboratory incubations demonstrated that As release from river muds at other locations can reach rates of >500 µM yr^{-1} (ref. [24]). These model-identified As release rates need to be understood in the context of river geomorphology[10]. The upstream end of our study site, that is, the location at which the river-water intrusion occurs, is located within an active depositional environment that contains highly reactive OM and results in a high net As release rate (Fig. 2). In contrast, aquifer sections located adjacent to erosional riverine environments were shown to be dominated by older sediments of lower reactivity and net As release[10].

Biogeochemical hotspots are defined as "areas that show disproportionately high reaction rates relative to the surrounding area"[27]. They emerge (1) where a convergence of flow paths and mixing of reactants occurs or (2) at terrestrial–aquatic interfaces through which hydrological flow paths carry a reactant into an adjacent zone in which a substrate (immobile) resides[27]. In our case, the large-scale groundwater abstractions of Hanoi's waterworks have altered the hydrological flow paths by inducing an advective flux of surface water across the bed of the Red River into the Holocene aquifer to create a new hotspot for As release. In the context of carbon and nitrogen cycling, river muds have previously been recognized as important BHRs in which terrestrial–aquatic interfaces are characterized by high biogeochemical turnover rates[27–29].

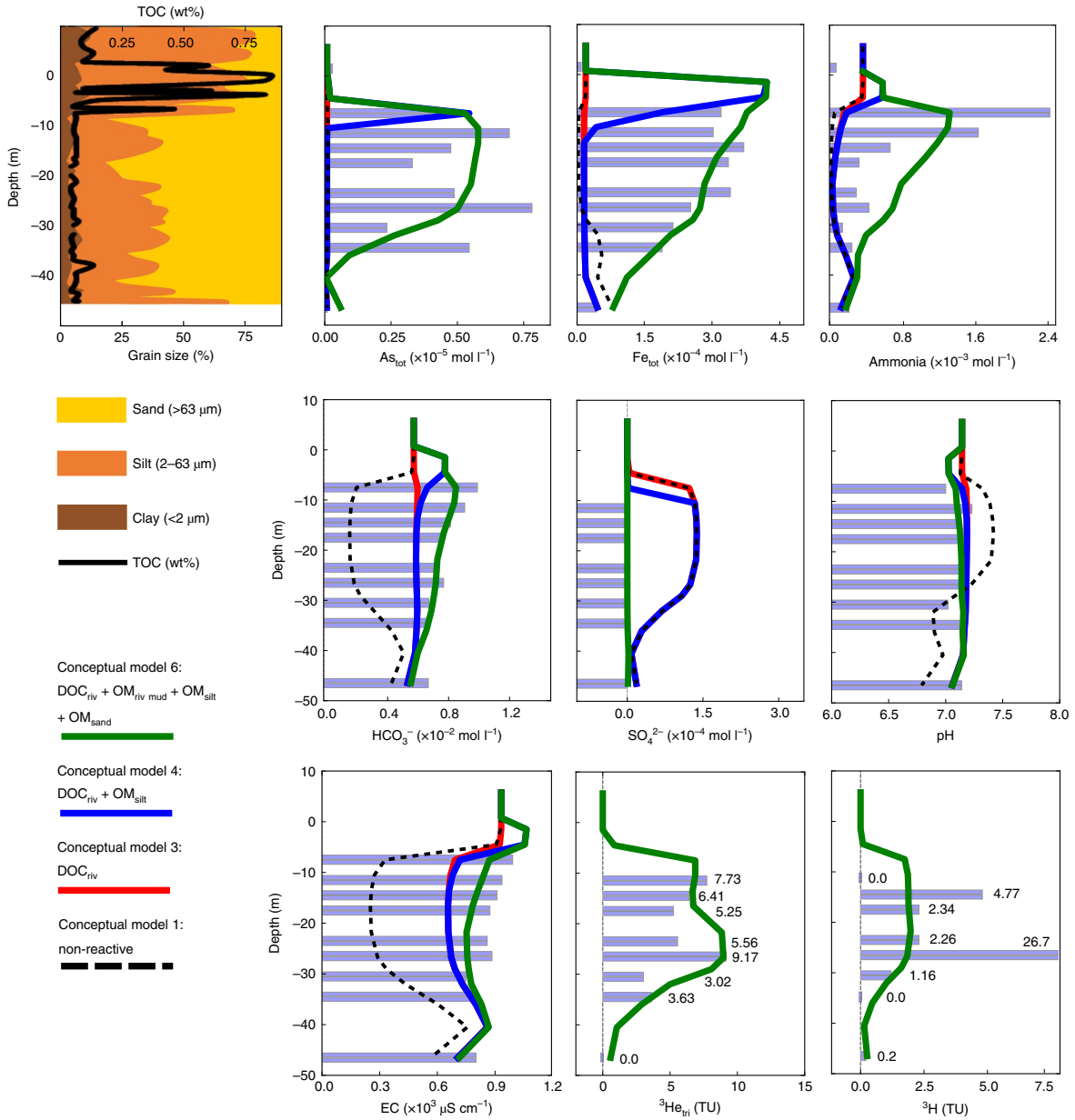

Fig. 5 | Observed and simulated depth profiles of concentrations, EC and pH. Observed (blue bars) and simulated (coloured lines) depth profiles of EC, pH and redox sensitive ions at site VPNS2 (Fig. 1) in 2010. Observed and simulated ^{3}H and ^{3}He$_{tri}$ concentrations are also shown as well as grain size (0–100%) and total organic carbon (TOC) distribution (0–1 wt%). Simulated data illustrate the different OM source terms and their effect on concentration patterns. DOC$_{riv}$, riverine OM; OM$_{silt}$, sediment OM in silt/clay; OM$_{riv\ mud}$, sediment OM in river muds; OM$_{sand}$, sediment OM in Holocene sands.

Our study shows and quantifies that the formation of As hotspots is facilitated by (1) the continuous co-deposition of labile organic carbon and As-hosting reactive Fe oxides in depositional zones along the river bank and (2) an advective flux that draws As-enriched pore water at the river–groundwater interface deeper into the aquifer. Substantial As release, however, only occurs when the flux of soluble electron acceptors supplied by the river water is consumed rapidly enough by the labile OM to allow for the occurrence of Fe-reducing conditions. Similar hotspots are also expected to develop at the interface between aquifers and geomorphic features, such as wetlands[14,16], ponds and irrigation channels[15], where labile material is replenished, effective hydrological pathways exist and the timescales of electron donor and acceptor consumption favour the establishment of Fe-reducing conditions. Otherwise, features such as buried peat layers or organic-rich clays may not act as hotspots if their low hydraulic conductivity prevents the rapid delivery of reactants. In such cases, mass fluxes into and from these features remain low. For the Van Phuc site, this is illustrated by the model-based estimate that the organic-rich clay layer, which overlies the Holocene aquifer, has contributed <5% to the overall As plume mass (Fig. 2 and Supplementary Table 4).

The complex hydrogeochemical interactions that can be addressed by our numerical framework are illustrated in Fig. 6. It summarizes the prerequisites and the varying influences of these key factors on the emergence of As hotspots as well as the geomorphological controls on their lifetime. The modelling results show that the sensitivity of As plume formation and the release dynamics of As are a function of four key factors: (1) OM abundance and/or reactivity (Fig. 6a), (2) Fe oxide abundance and/or reactivity (Fig. 6b), (3) advective flow

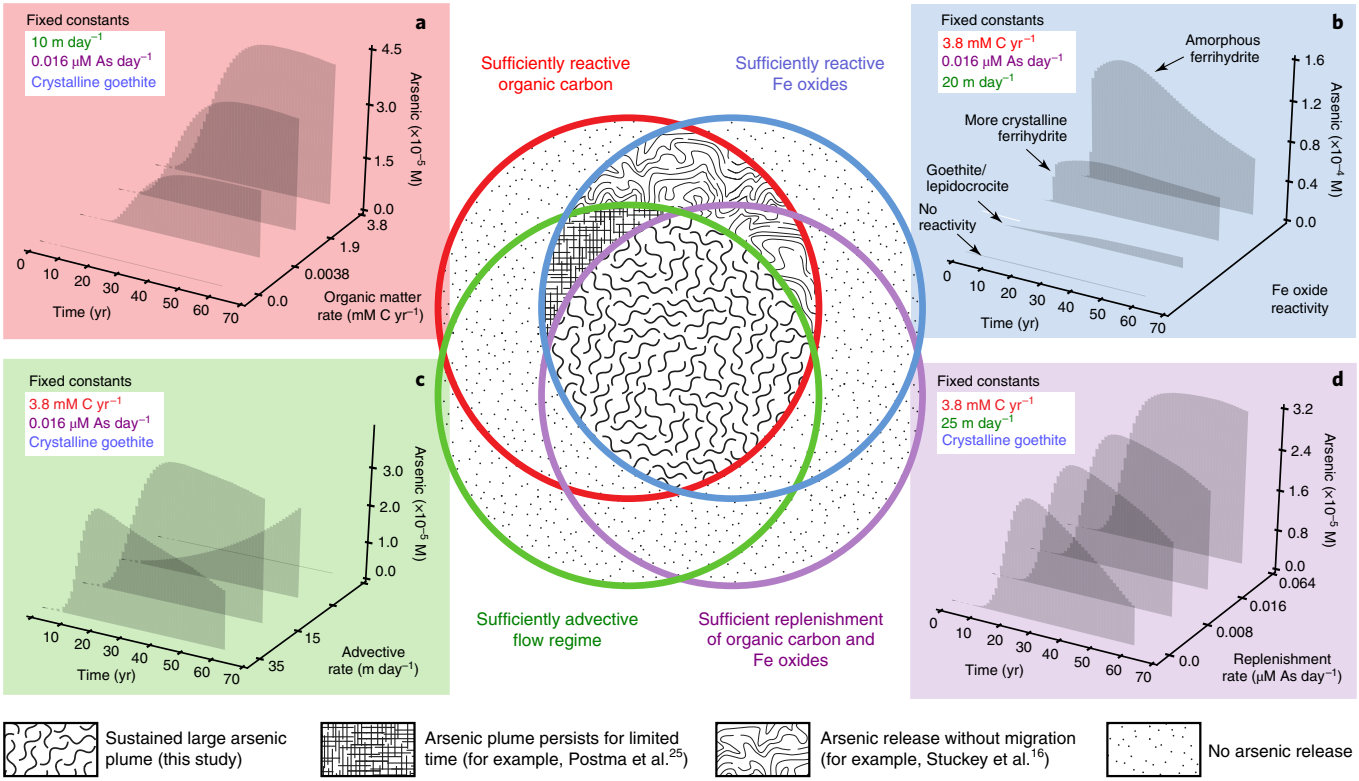

Fig. 6 | Model-computed sensitivities of As plume formation at biogeochemical reaction hotspots. a–d, Sustained As plumes rely on the co-occurrence of labile organic carbon (**a**), reactive As-hosting Fe oxides (**b**), advection of As-enriched pore waters (**c**) and a continuous replenishment of organic carbon and As-hosting Fe oxides (**d**). The ratio between advection and As release rates determines the As levels. The joint occurrence or partial absence of **a–d** controls the impact of typical As sources, such as ponds and channels[15], wetlands[14,30], buried peat layers[4,12] and fractured organic-rich clay deposits[14,26]. For example, where replenishment (**d**) is absent, such as in non-depositional river sections[25], a BRH occurs only temporarily ('hot moment')[27]. Static As pollution occurs where advection (**c**) is absent, such as in clay-occupied sections at Van Phuc or low-conductivity aquifers below ponds[16].

rates (Fig. 6c) and (4) river-mud deposition rate (Fig. 6d). It is also suggested that, in the absence of a sufficiently high river-mud replenishment rate, only an As 'hot moment'[27] develops with an initial As release peak followed by successively decreasing As concentrations at the river–groundwater interface.

Overlooking the critical role of flow and solute transport explains why many As-affected areas have failed to exhibit a relationship between sediment-bound and dissolved As concentrations. This is why hydraulic, hydrological and biogeochemical processes must be explicitly considered and integrated to explain the variability of As concentrations within and between aquifers. For the investigated site, we have shown how integrated flow and reactive transport modelling has facilitated a more precise, mechanistic understanding of the processes that control the dynamics of As concentration in space and time. Such a mechanistic understanding and its translation into process-based models to frame As migration rates is crucial for the development of safe and sustainable water management strategies.

Online content

Any methods, additional references, Nature Research reporting summaries, source data, extended data, supplementary information, acknowledgements, peer review information; details of author contributions and competing interests; and statements of data and code availability are available at https://doi.org/10.1038/s41561-020-0557-6.

Received: 16 December 2018; Accepted: 19 February 2020;
Published online: 07 April 2020

References

1. Fendorf, S., Michael, H. A. & van Geen, A. Spatial and temporal variations of groundwater arsenic in South and Southeast Asia. *Science* **328**, 1123–1127 (2010).
2. Winkel, L. H. et al. Arsenic pollution of groundwater in Vietnam exacerbated by deep aquifer exploitation for more than a century. *Proc. Natl Acad. Sci.* **108**, 1246–1251 (2011).
3. Postma, D. et al. Groundwater arsenic concentrations in Vietnam controlled by sediment age. *Nat. Geosci.* **5**, 656–661 (2012).
4. Berg, M. et al. Hydrological and sedimentary controls leading to arsenic contamination of groundwater in the Hanoi area, Vietnam: the impact of iron–arsenic ratios, peat, river bank deposits, and excessive groundwater abstraction. *Chem. Geol.* **249**, 91–112 (2008).
5. Radloff, K. et al. Reversible adsorption and flushing of arsenic in a shallow, Holocene aquifer of Bangladesh. *Appl. Geochem.* **77**, 142–157 (2017).
6. Neumann, R. B. et al. Anthropogenic influences on groundwater arsenic concentrations in Bangladesh. *Nat. Geosci.* **3**, 46–52 (2010).
7. van Geen, A. et al. Retardation of arsenic transport through a Pleistocene aquifer. *Nature* **501**, 204–207 (2013).
8. Khan, M. R. et al. Megacity pumping and preferential flow threaten groundwater quality. *Nat. Commun.* **7**, 12833 (2016).
9. Michael, H. A. & Khan, M. R. Impacts of physical and chemical aquifer heterogeneity on basin-scale solute transport: vulnerability of deep groundwater to arsenic contamination in Bangladesh. *Adv. Water Resour.* **98**, 147–158 (2016).
10. Stahl, M. O. et al. River bank geomorphology controls groundwater arsenic concentrations in aquifers adjacent to the Red River, Hanoi Vietnam. *Water Resour. Res.* **52**, 6321–6334 (2016).
11. McArthur, J., Ravenscroft, P., Safiulla, S. & Thirlwall, M. Arsenic in groundwater: testing pollution mechanisms for sedimentary aquifers in Bangladesh. *Water Resour. Res.* **37**, 109–117 (2001).
12. McArthur, J. et al. Natural organic matter in sedimentary basins and its relation to arsenic in anoxic ground water: the example of West Bengal and its worldwide implications. *Appl. Geochem.* **19**, 1255–1293 (2004).

13. Meharg, A. A. et al. Codeposition of organic carbon and arsenic in Bengal Delta aquifers. *Environ. Sci. Technol.* **40**, 4928–4935 (2006).
14. Postma, D. et al. Arsenic in groundwater of the Red River floodplain, Vietnam: controlling geochemical processes and reactive transport modeling. *Geochim. Cosmochim. Acta* **71**, 5054–5071 (2007).
15. Polizzotto, M. L., Kocar, B. D., Benner, S. G., Sampson, M. & Fendorf, S. Near-surface wetland sediments as a source of arsenic release to ground water in Asia. *Nature* **454**, 505–509 (2008).
16. Stuckey, J. W., Schaefer, M. V., Kocar, B. D., Benner, S. G. & Fendorf, S. Arsenic release metabolically limited to permanently water-saturated soil in Mekong Delta. *Nat. Geosci.* **9**, 70–76 (2016).
17. Berg, M. et al. Arsenic contamination of groundwater and drinking water in Vietnam: a human health threat. *Environ. Sci. Technol.* **35**, 2621–2626 (2001).
18. Harvey, C. F. et al. Arsenic mobility and groundwater extraction in Bangladesh. *Science* **298**, 1602–1606 (2002).
19. Horneman, A. et al. Decoupling of As and Fe release to Bangladesh groundwater under reducing conditions. Part 1: Evidence from sediment profiles. *Geochim. Cosmochim. Acta* **68**, 3459–3473 (2004).
20. Islam, F. S. et al. Role of metal-reducing bacteria in arsenic release from Bengal delta sediments. *Nature* **430**, 68–71 (2004).
21. Eiche, E. *Arsenic Mobilization Processes in the Red River Delta, Vietnam: Towards a Better Understanding of the Patchy Distribution of Dissolved Arsenic in Alluvial Deposits* (Karlsruher Mineralogische und Geochemische Hefte 37, KIT Scientific, 2009).
22. Frei, F. *Groundwater Dynamics and Arsenic Mobilization near Hanoi (Vietnam) Assessed Using Noble Gases and Tritium* Diploma Thesis, ETH Swiss Federal Institute of Technology, Department of Environmental Sciences (2007).
23. Eiche, E. et al. Origin and availability of organic matter leading to arsenic mobilisation in aquifers of the Red River Delta, Vietnam. *Appl. Geochem.* **77**, 184–193 (2017).
24. Postma, D. et al. Mobilization of arsenic and iron from Red River floodplain sediments, Vietnam. *Geochim. Cosmochim. Acta* **74**, 3367–3381 (2010).
25. Postma, D. et al. Fate of arsenic during Red River water infiltration into aquifers beneath Hanoi, Vietnam. *Environ. Sci. Technol.* **51**, 838–845 (2017).
26. Larsen, F. et al. Controlling geological and hydrogeological processes in an arsenic contaminated aquifer on the Red River flood plain, Vietnam. *Appl. Geochem.* **23**, 3099–3115 (2008).
27. McClain, M. E. et al. Biogeochemical hot spots and hot moments at the interface of terrestrial and aquatic ecosystems. *Ecosystems* **6**, 301–312 (2003).
28. Cheng, F. Y. & Basu, N. B. Biogeochemical hotspots: role of small water bodies in landscape nutrient processing. *Water Resour. Res.* **53**, 5038–5056 (2017).
29. Hedin, L. O. et al. Thermodynamic constraints on nitrogen transformations and other biogeochemical processes at soil–stream interfaces. *Ecology* **79**, 684–703 (1998).
30. Kocar, B. D. & Fendorf, S. in *Interdisciplinary Studies on Environmental Chemistry—Environmental Pollution and Ecotoxicology* (eds Kawaguchi, M. et al.) 117–124 (TERRAPUB, 2012).

Methods

Field site. The study site is located near the village of Van Phuc (10 km southeast of Hanoi, Vietnam) where As pollution has been investigated since 2001. The general lithological, hydrological and geochemical characteristics of the site are well-known from previous studies[4,7,10,31–34]. A special feature of Van Phuc is that the advection of groundwater is induced by massive groundwater withdrawal for the municipal water supply of Hanoi[2,4,7]. However, the site displays typical conditions of As-polluted Holocene and Pleistocene aquifers in south and southeast Asia with deposited sediments being of a similar origin and depositional environment as those of the floodplain sediments along the Mekong, Ganges and Brahmaputra deltas in Cambodia, Bangladesh and West Bengal. The general stratigraphy is heterogeneous and marked by intercalations of fine-to-coarse Holocene sands with a burial age of <5,000 yr, which are in lateral contact with Pleistocene sands, silts and gravels that were deposited >12,000 years ago (van Geen et al.[7]). These are overlain by a confining clay and silt layer 10–20 m thick (Fig. 1). Important examples of other well-studied sites that share similar characteristics include Araihazar (Meghna River, Bangladesh (for example, van Geen et al.[35])), Munshiganj (Ganges River, Bangladesh (for example, Harvey et al.[18])), Barasat (Hoogli River, West Bengal (for example, McArthur et al.[36])) or Dan Phuong (Red River, Vietnam (for example, Postma et al.[14]).

Owing to the large-scale groundwater abstraction at the Hanoi water works, the study site benefits from relatively well-controlled hydraulic flow conditions with groundwater flow directions directed consistently towards a cone of depression beneath Hanoi. This site therefore provides a unique opportunity to determine As migration rates over several decades, which is a substantial advantage over many other As-affected locations, at which the historic groundwater flow conditions remain far less determined and are often far more complex.

Modelling approaches and tools. Based on the hydrogeological site characterization, environmental tracer data and the records of observed aqueous and solid phase chemistry, we formulated a wide range of plausible conceptual models for both the physical processes (flow and non-reactive transport) and the geochemical processes. Each of the conceptual models was translated into a corresponding numerical model. The US Geological Survey (USGS) flow model MODFLOW[37] was used to perform the groundwater flow simulations, and the reactive multicomponent transport model PHT3D[38] was used to simulate the solute and reactive transport processes. PHT3D couples the 3D transport simulator MT3DMS[39] with the USGS geochemical model PHREEQC-2[40]. The model development was performed in two phases. The first phase focused on developing an understanding and quantification of the flow and solute transport behaviour. Measured environmental tracer data for ^3H and $^3He_{tri}$ were used as a model calibration target to reproduce the historic groundwater flow rates at the study site as accurately as possible. The second phase focused on the identification and quantification of the biogeochemical processes and the analysis of the most plausible conceptual model for the site's reactive transport processes. This included the investigation of different conceptual model variants (CM1 to CM6 (Extended Data Table 1)). The PEST++ software[41] was then used to conduct the calibration phase in parallel via transmission control protocol/internet protocol network communications to achieve a joint calibration of flow, solute and reactive transport parameters.

Model set-up. Based on previous investigations (for example, van Geen et al.[7]) that showed a relatively constant flow direction, the numerical models were constructed as a 2D vertical transect model. The model domain was aligned with the main groundwater flow direction observed in the Pleistocene and Holocene aquifer, that is, from the southeast to northwest (Fig. 1). Overall, the selected model domain covers a lateral flow distance of 2.78 km, originating at the SW river bank. The selected transect passes several monitoring boreholes and includes two multilevel monitoring devices (VPNS1 and VPNS2) for which high-resolution concentration depth profiles are available (Supplementary Figs. 1, 3 and 4).

The Holocene and Pleistocene aquifers, which include an overlying clay and silt aquitard section, were discretized into 15 model layers to obtain a sufficiently high vertical resolution of the biogeochemical gradients. The simulation period was set to 60 yr, commencing in January 1950, that is, before groundwater abstraction in Hanoi started and before bomb-derived ^3H concentrations impacted groundwater and surface water concentrations. To represent (1) the variations of atmospheric ^3H concentrations and the corresponding variations in the Red River and (2) the successively changing groundwater flow regime that can be attributed to groundwater extractions in Hanoi, the simulation time was discretized into 12 hydraulically and/or hydrochemically differing stress periods of length 5 yr (Supplementary Fig. 2).

Implementation of environmental tracer transport. The transient flow model was calibrated based on measured ^3H and $^3He_{tri}$ concentrations to replicate the observed groundwater age distribution at the site. ^3H input to the model was based on the atmospheric ^3H values reported by the International Atomic Energy Agency for Hong Kong (Global Network of Isotopes in Precipitation King's Park station; https://nucleus.iaea.org/) and assigned as time-varying specified concentrations to all the model grid cells that represent the Red River. ^3H decay and the production of $^3He_{tri}$ during advective–dispersive transport was considered through a first-order rate reaction using a half-life of 12.32 yr, according to:

$$\frac{dC_{^3H}}{dt} = -k_{^3H}\, C_{^3H}\,, \frac{dC_{^3He_{tri}}}{dt} = +k_{^3H}\, C_{^3H}$$

where $C_{^3H}$ and $C_{^3He_{tri}}$ are the ^3H and $^3He_{tri}$ concentrations and $k_{^3H}$ is the first-order rate constant.

Biogeochemical reaction network. Building on the calibrated groundwater flow and solute transport model, the subsequent reactive transport simulations were performed to interpret the hydrochemical observations at Van Phuc. Through the model-based analysis of field observations, which included both the identification of the most plausible conceptual model and the estimation of suitable and plausible model parameters, a mechanistic understanding of the As distribution patterns and of their evolution was derived. The reactive transport model incorporated the mineralogical data that were previously collected for the Holocene sediments along with observed or reconstructed water compositions (Extended Data Tables 2 and 3). Based on the available data, the reaction network was defined and then successively refined until the observations could be reproduced. The defined reaction network considered the key biogeochemical processes that were hypothesized to govern the major ion and redox chemistry as well as the partitioning behaviours of the trace constituents, such as As and phosphate, between the pore water and sediments. The most important biogeochemical process was the oxidation of DOC and SOM, coupled to the reduction of various electron acceptors. At Van Phuc, DOC and SOM mineralization occurred under aerobic, denitrifying, sulfate-reducing and Fe(III)-reducing conditions. These reactions were considered in the model through a partial equilibrium approach, which assumes that the oxidation step is the rate-limiting step (for example, Postma and Jakobsen[42]). Consistent with previous, closely related studies (for example, Prommer et al.[43], Sharma et al.[44] and Rawson et al.[45]) the computed rates of OM mineralization depended on the abundance of multiple electron acceptors:

$$r_{OM} = k_{ox}\left(\frac{C_{ox}}{2.9\times10^{-4}+C_{ox}}\right) + k_{nitr}\left(\frac{C_{nitr}}{1.55\times10^{-4}+C_{nitr}}\right)\times\left(\frac{k_{ox,inh}}{k_{ox,inh}+C_{ox}}\right) + k_{sul}\left(\frac{C_{sul}}{1.0\times10^{-4}+C_{sul}}\right)\times\left(\frac{k_{ox,inh}}{k_{ox,inh}+C_{ox}}\right)\times\left(\frac{k_{nitr,inh}}{k_{nitr,inh}+C_{nitr}}\right) + k_{Fe}\left(\frac{C_{Fe}}{1.0\times10^{-6}+C_{Fe}}\right)$$

where r_{OM} is the overall degradation rate of OM, k_{ox}, k_{nitr}, k_{sul} and k_{Fe} are the maximum rate constants for OM mineralization under aerobic, denitrifying, sulfate- and Fe(III)-reducing conditions. C_{ox}, C_{nitr}, C_{sul} and C_{Fe} are the concentrations of dissolved oxygen, nitrate, sulfate and Fe(III) oxides, respectively, and $k_{ox,inh}$ and $k_{nitr,inh}$ are inhibition constants. The reactivity of the different OM sources within the aquifer, that is, young OM in river muds, OM in sand and clay/silt deposits and DOC within the intruding river water, was determined through the automatic model calibration procedure. A generic stoichiometric composition of $(CH_2O)_{106}(NH_3)_{11}(H_3PO_4)_4$ was assumed for both DOC and SOM[21].

Calcite and Fe(III) oxides were included in the reaction network as the main minerals that affect the study site's hydrochemical compositions. The exact nature of the Fe(III) oxides at the site is unknown. A single Fe(III)-oxide phase, represented as $Fe(OH)_3$, was therefore used in the model for simplicity. The solubility of this Fe(III) oxide, expressed as $K = [Fe^{3+}]/[H^+]^3$, was determined as part of the PEST++ model calibration procedure. The estimated log K of +0.23 (Supplementary Table 5) corresponds to a microcrystalline goethite[46]. This is consistent with previously determined solubilities for Fe(III) oxides in a Holocene sand aquifer 30 km north of Hanoi along the Red River by Postma et al.[24], which ranged from lepidocrocite and/or poorly crystalline goethite to haematite. It is also consistent with a sequential extraction analysis from the Van Phuc site, which suggested that the dominant non-silicate Fe phase in the Holocene sediments was goethite and/or haematite[32].

Replenishment of iron oxides at the river–aquifer interface was included in the model through a zeroth-order rate expression, which replenishes the Fe(III)-oxide pool at a constant rate, consistent with the location of the field site in a depositional environment. The zeroth-order rate constant was included as an adjustable parameter in the automatic model calibration to obtain an estimate for the replenishment rate (Supplementary Table 5). The composition of the iron oxide was defined to contain As(V) at an As/Fe molar ratio of 2 mmol mol^{-1}. This is in agreement with Postma et al.[24], who obtained As/Fe ratios between 1 and 2 mmol mol^{-1} for river sand material obtained from floodplains in Vietnam during laboratory extraction experiments.

The sorption of As in the Holocene section of the aquifer was assumed to occur on the surfaces of Fe(III) oxides. In the model, the total number of sorption sites on the Fe(III) oxides was stoichiometrically linked with simulated Fe(III) oxide concentrations. By doing so, the successively decreasing sorption capacity that results from the reductive dissolution of Fe(III) oxides was considered[47]. In addition, As can also be liberated as a result of competitive displacement from sorption sites. Sequential extraction analysis by Berg et al.[4] and Eiche et al.[21]

showed easily desorbable As to be the by far dominant pool of As throughout the aquifer at the site (Supplementary Fig. 1). To allow for a process-based description of competitive sorption effects and the influence from pH changes on As dynamics, surface complexation models were employed. The generalized two-layer surface complexation model of Dzombak and Morel[48] was considered in the reaction network, extended by reactions for Fe^{2+}, HCO_3^- and Si with reaction constants adopted from the literature[47–49]. The densities of strong and weak sites on the Fe(III) oxides were included as adjustable parameters within the automatic model calibration procedure. For the Pleistocene section of the aquifer, the recently developed generalized surface complexation model of Rathi et al[31] was employed for As and P.

Initial and boundary conditions. The water compositions that were employed to define the initial concentrations in the model simulations were based on the hydrochemical data collected by Frei[22] and van Geen et al.[7] and through two field campaigns in September 2006 and April 2010 (Extended Data Table 2 and Supplementary Tables 1 and 2). The initial water composition that was attributed to the Holocene aquifer section of the model was taken from monitoring borehole VPNS4, located about 1.9 km distance from the Red River. The groundwater from this site was analysed as being old (that is, prebomb) and therefore presumably unaffected by any geochemical changes that could have occurred as a result of the hydrological changes induced since 1950. However, the assumed initial dissolved As and phosphate concentrations were increased from the measured concentrations to match the measured sorbed As and phosphate concentration ranges in the aquifer sediments and river-bed deposits. The portioning between the sorbed and aqueous phase is thereby determined through the electrostatic double-layer model (Extended Data Table 3). The water composition that persisted in the gravel layer (Fig. 2) that underlies the Holocene and Pleistocene sands differed from that of the sands and was established on the basis of three sampled horizons with depths >54 m, which accessed the gravel (Extended Data Table 2). The water composition attributed to model grid cells that represent the Red River was based on hydrochemical measurements for the Red River, except for ^3H. The ^3H concentrations were defined in accordance with the time-variant atmospheric ^3H values that were reported for Hong Kong (Global Network of Isotopes in Precipitation King's Park station). All the assumed initial concentrations were charge balanced and equilibrated with respect to the prevailing mineral composition. The assumed initial mineral concentrations in the model simulations were based on the results of earlier sediment analysis[7,10,21] (Extended Data Table 3).

Model calibration procedure. The groundwater flow and reactive transport model was calibrated using the non-linear regression software PEST, which was implemented in parallel on high-performance computing systems via PEST++[41]. The flow and solute transport calibration dataset consisted primarily of the measured $^3He_{tri}$ and ^3H concentrations, along with a hydraulic gradient observation, which was based on the average measured water levels between two monitoring bores, AMS12 and AMS16 (Fig. 1). The composite weighted sum of squared residuals (that is, differences between the observed quantities and their model-simulated equivalents) was used as the primary objective function to be minimized during the calibration process.

There were a total of 18 ^3H and 19 $^3He_{tri}$ observations available from various depths; all observations were obtained in 2007[7,22]. The weights imposed on each observation of ^3H and $^3He_{tri}$ were generally set to 1.0, with some weights being slightly adjusted to reflect their potential inherent measurement and model-structure errors. As the hydraulic gradient observation had a smaller magnitude (about 1–3 orders) and consisted of only a single observation, it was assigned a weight of 1×10^5 such that it produced a relatively comparable contribution to the composite least-squares objective function.

Estimated model parameters consisted of horizontal and vertical hydraulic conductivity, porosity and the conductance of the general-head boundary condition. The hydraulic conductivity and porosity were parameterized using a zonation method, which resulted in 9 zones for each of the 3 parameter types (Supplementary Fig. 4), that is, a total of 28 estimated hydrological parameters.

Owing to the relatively high degree of parameterization, the inverse problem was underdetermined. Tikhonov regularization was employed to alleviate overparameterization by incorporating prior information, an approximate Bayesian approach[41]. This prior information consisted of an expected vertical anisotropy of 100 for hydraulic conductivity, and a tendency towards homogeneous conditions for porosity values assigned to zones with similar aquifer materials (for example, zones within the Holocene sediments have a tendency towards similar porosity values).

The geochemical parameters were calibrated jointly with the flow and solute parameters. Although the larger-scale groundwater flow and transport patterns in the Holocene aquifer show a truly 3D behaviour, the simulation of the reactive transport of solutes along the selected vertical transect is thought to be an adequate approximation. Where important hydrochemical data required to fill 'data gaps' were not collected from wells that resided directly on the modelled transect but in its vicinity (Fig. 1), we projected these observations onto the selected transect (AMS15 and VPNS9 (Fig. 3)).

The joint calibration of flow, solute and reactive transport parameters allowed the most appropriate conceptual model replicating the observed flow and geochemical field data to be revealed as part of the model calibration process. For the conceptual model that produces the smallest objective function value, the calibrated hydrochemical and flow/transport parameters are listed in Supplementary Tables 5 and 6. These tables also list the parameter bounds and the posterior uncertainty statistics as per the GENLINPRED procedure provided in the PEST software suite, which considers both Bayesian and subspace-based methodologies.

Investigated model variants. We investigated a suite of plausible conceptual and numerical model variants for the site's reactive transport processes (conceptual model variants CM1 to CM6 (Extended Data Table 1)). Variant CM6 provided a numerical implementation that included, besides a comprehensive range of biogeochemical reactions, the entire range of potential OM sources within the investigated groundwater system and served as the basis for the inversion process. The systematic comparison between model simulation results and observations thereby allowed for the process-based model to reveal independently whether a process contributed to the field-observed hydrochemical patterns, that is, the spatial distribution of major ion compositions, redox conditions and in particular As concentrations. The inversion process revealed that OM sources at the study site had distinctively different reactivities depending on their lithological association, which was explored and illustrated further through model variants CM1 to CM5:

- CM1: non-reactive model variant that allows us to illustrate the impact of geochemical reactions and to distinguish between transport and reaction-derived concentration changes
- CM2: model variant without any OM source that demonstrates the importance of OM mineralization compared to that of other reactive processes in liberating As
- CM3: model variant that assumes DOC to be the sole OM source and illustrates that the DOC from intruding river water alone is insufficient to achieve the observed electron-acceptor consumption and associated secondary geochemical reaction patterns
- CM4 to CM5: conceptual models that include DOC and SOM but differ in relation to the distribution of the SOM within the aquifer. These model variants illustrate the effect of OM sources and mineralization rates on concentration patterns, including:
  - the importance of vertical As mass transfer into the Holocene aquifer from the clay/silt deposits
  - the contribution of aquifer in situ liberation of As
  - the significance of the river-mud deposits for As mobilization at the site.

Model uncertainty. The lack of long-term historical water level and concentration data, especially from the period prior to the reversal of the hydraulic gradient, is a source of model uncertainty. For example, time series of hydraulic head data, which document the deepening of the cone of depression due to increased groundwater abstractions at the Hanoi water works, are scarce. However, this lack of data is largely compensated by the use of age-tracer concentrations as additional constraints for the groundwater flow model simulations. These measured environmental tracer concentrations provide a time-integrated measure of river-water intrusion. Furthermore, our model-derived interpretation of the regional scale concentration patterns establishes the importance of the river–groundwater interface as a geochemical reaction hotspot. Clearly, the numerical implementation of the interface is, despite the consideration of many process details, still idealized due to the (large) scale of the model domain and the lack of spatially more dense observation data in the proximity of the interface. Future, more detailed investigations of this zone will allow us to reveal additional process details and to more tightly constrain the model simulations of the interface processes.

Data availability

The geochemical data analysed during this study are included in this article in the supplementary information in Supplementary Tables 1 and Supplementary Tables 2. The groundwater age data analysed during this study has been published and is available in van Geen et al.[7] and Stahl et al.[10] (Supplementary Table 1). The solid phase chemistry data at the site was available from Eiche et al.[32] and Eiche[21].

Code availability

All codes used as part of this study are publicly available and can be accessed freely. The USGS flow model MODFLOW[37] (https://www.usgs.gov/software/software-modflow) was used to perform the groundwater flow simulations, whereas the reactive multi-component transport model PHT3D[38] was used to simulate solute and reactive transport processes (http://www.pht3d.org/). PHT3D couples the 3D transport simulator MT3DMS[39] with the USGS geochemical model PHREEQC-2[40].

The PEST++ software suite[41] was employed for model calibration and uncertainty analysis (http://www.pesthomepage.org/).

References

31. Rathi, B., Neidhardt, H., Berg, M., Siade, A. & Prommer, H. Processes governing arsenic retardation on Pleistocene sediments: adsorption experiments and model-based analysis. *Water Resour. Res.* **53**, 4344–4360 (2017).
32. Eiche, E. et al. Geochemical processes underlying a sharp contrast in groundwater arsenic concentrations in a village on the Red River delta, Vietnam. *Appl. Geochem.* **23**, 3143–3154 (2008).
33. van Geen, A. et al. Comparison of arsenic concentrations in simultaneously-collected groundwater and aquifer particles from Bangladesh, India, Vietnam, and Nepal. *Appl. Geochem.* **23**, 3244–3251 (2008).
34. Neidhardt, H. et al. Insights into arsenic retention dynamics of Pleistocene aquifer sediments by in situ sorption experiments. *Water Res.* **129**, 123–132 (2018).
35. van Geen, A. et al. Spatial variability of arsenic in 6000 tube wells in a 250 km^2 area of Bangladesh. *Water Resour. Res.* **39**, 1140 (2003).
36. McArthur, J. et al. How paleosols influence groundwater flow and arsenic pollution: a model from the Bengal Basin and its worldwide implication. *Water Resour. Res.* **44**, W11411 (2008).
37. Harbaugh, A. W. *MODFLOW-2005, the US Geological Survey Modular Ground-water Model: The Ground-water Flow Process* (US Department of the Interior, US Geological Survey, 2005).
38. Prommer, H., Barry, D. A. & Zheng, C. MODFLOW/MT3DMS-based reactive multicomponent transport modeling. *Ground Water* **41**, 247–257 (2003).
39. Zheng, C. & Wang, P. P. *MT3DMS: A Modular Three-dimensional Multispecies Transport Model for Simulation of Advection, Dispersion, and Chemical Reactions of Contaminants in Groundwater Systems; Documentation and User's Guide* (U.S. Army Corps of Engineers Document, 1999).
40. Parkhurst, D. L. & Appelo, C. *User's Guide to PHREEQC (Version 2): A Computer Program for Speciation, Batch-Reaction, One-Dimensional Transport, and Inverse Geochemical Calculations* Report No. 99-4259 (USGS, 1999).
41. Welter, D. E., White, J. T., Hunt, R. J. & Doherty, J. E. *Approaches in Highly Parameterized Inversion—PEST++ Version 3, a Parameter ESTimation and Uncertainty Analysis Software Suite Optimized for Large Environmental Models* Report No. 2328-7055 (USGS, 2015).
42. Postma, D. & Jakobsen, R. Redox zonation: equilibrium constraints on the Fe(III)/SO_4-reduction interface. *Geochim. Cosmochim. Acta* **60**, 3169–3175 (1996).
43. Prommer, H., Tuxen, N. & Bjerg, P. L. Fringe-controlled natural attenuation of phenoxy acids in a landfill plume: integration of field-scale processes by reactive transport modeling. *Environ. Sci. Technol.* **40**, 4732–4738 (2006).
44. Sharma, L., Greskowiak, J., Ray, C., Eckert, P. & Prommer, H. Elucidating temperature effects on seasonal variations of biogeochemical turnover rates during riverbank filtration. *J. Hydrol.* **428**, 104–115 (2012).
45. Rawson, J. et al. Quantifying reactive transport processes governing arsenic mobility after injection of reactive organic carbon into a Bengal Delta aquifer. *Environ. Sci. Technol.* **51**, 8471–8480 (2017).
46. Schwertmann, U. Solubility and dissolution of iron oxides. *Plant Soil* **130**, 1–25 (1991).
47. Appelo, C. A. J., Van der Weiden, M. J. J., Tournassat, C. & Charlet, L. Surface complexation of ferrous iron and carbonate on ferrihydrite and the mobilization of arsenic. *Environ. Sci. Technol.* **36**, 3096–3103 (2002).
48. Dzombak, D. A. & Morel, F. M. *Surface Complexation Modeling: Hydrous Ferric Oxide* (John Wiley & Sons, 1990).
49. Swedlund, P. J. & Webster, J. G. Adsorption and polymerisation of silicic acid on ferrihydrite, and its effect on arsenic adsorption. *Water Res.* **33**, 3413–3422 (1999).

Acknowledgements

This study was supported by the Swiss National Science Foundation (SNSF grant no. IZK0Z2_150435/ IZK0Z2_150435/1 and SNSF grant no. 167821) and the German Research Foundation (DFG grant no. 320059499). M. O. Stahl (Union College), B. Bostick and A. van Geen (Columbia University) contributed to this work through helpful discussions on previous work at the field site. P. Ortega prepared Fig. 1.

Author contributions

R.K., M.B., I.W. and H.P. conceived the study. M.B. and R.K. provided hydrochemical and tracer data and contributed to the groundwater age, hydraulic and hydrogeochemical interpretation. I.W. and H.P. carried out the flow and reactive transport modelling and J.S., M.B., R.K, I.W. and H.P. contributed to the development of the geochemical conceptual model underpinning the numerical model. A.J.S. undertook flow and solute transport model calibration and contributed to model uncertainty analysis. All authors contributed to writing and editing the paper.

Competing interests

The authors declare no competing interests.

Additional information

Extended data is available for this paper at https://doi.org/10.1038/s41561-020-0557-6.

Supplementary information is available for this paper at https://doi.org/10.1038/s41561-020-0557-6.

Correspondence and requests for materials should be addressed to I.W.

Peer review information Primary Handling Editors: Tamara Goldin; Melissa Plail.

Reprints and permissions information is available at www.nature.com/reprints.

Extended Data Table 1 | Conceptual and numerical model variants

Conceptual Model	Organic matter source				Core biogeochemical reactions common to CM2 to CM6
	Red River	**Clay/silt layer**	**Holocene sands**	**River-muds**	
	dissolved org. matter	*sed.-bound org. matter*	*sed.-bound org. matter*	*sed.-bound org. matter*	
CM 1	Non-reactive				N/A
CM 2	-	-	-	-	(i) organic matter mineralisation under aerobic, denitrifying, sulphate-reducing and Fe-reducing conditions; (ii) precipitation and reductive dissolution of Fe(III) oxides; (iii) calcite dissolution and precipitation and (iv) surface complexation reactions of arsenic and other ions onto Fe(III) oxides
CM 3	X	-	-	-	
CM 4	X	X		-	
CM 5	X	X	X		
CM 6	X	X	X	X	

Extended Data Table 2 | Measured and modelled initial (that is, native groundwater and river water) concentrations of aqueous components. Concentrations in mol/L except temperature in [°C], EC in [µS/cm] and pH, pe with bd = below detection limit

	River	Holocene Aquifer			Pleistocene Aquifer			Deep Pleistocene Gravel Aquifer		
	Model input	Model input [1)]	Measured range		Model input[3)]	Measured range		Model input	Measured range	
			min	Max		min	max		min	max
EC	-	-	436	1051	-	257	926	-	407	805
pH	7.4	7.1	6.4	7.4	6.8	6.2	7.1	6.8	6.2	7.14
pe	12.2	-3.3	-	-	-2.8	-	-	-2.8	-	-
temp	28	25.3	24.9	27.7	25.3	25.1	26.8	25.3	25.1	25.9
HCO_3^-	1.9×10^{-3}	6.4×10^{-3}	4.1×10^{-3}	1.3×10^{-2}	4.4×10^{-3}	2.3×10^{-3}	8.8×10^{-3}	5.1×10^{-3}	3.4×10^{-3}	6.9×10^{-3}
Ca	7.6×10^{-4}	2.8×10^{-3}	6.2×10^{-4}	3.2×10^{-3}	6.4×10^{-4}	1.9×10^{-4}	2.8×10^{-3}	1.5×10^{-3}	6.1×10^{-4}	2.8×10^{-3}
Mg	2.5×10^{-4}	1.5×10^{-3}	7.3×10^{-4}	1.6×10^{-3}	9.6×10^{-4}	3.8×10^{-4}	1.9×10^{-3}	8.4×10^{-4}	3.9×10^{-4}	1.2×10^{-3}
Cl[2)]	2.2×10^{-4}	3.3×10^{-3}	7.0×10^{-6}	4.9×10^{-4}	7.4×10^{-4}	6.1×10^{-5}	2.1×10^{-4}	1.5×10^{-3}	6.2×10^{-5}	1.5×10^{-4}
Na	3.9×10^{-4}	7×10^{-4}	2.6×10^{-4}	8.6×10^{-4}	1.1×10^{-3}	4.6×10^{-4}	1.6×10^{-3}	9.4×10^{-4}	5.1×10^{-4}	1.4×10^{-3}
K	7.9×10^{-5}	1.3×10^{-4}	3×10^{-5}	4.3×10^{-4}	7.9×10^{-5}	5.1×10^{-5}	5.1×10^{-4}	2.1×10^{-4}	6.9×10^{-5}	3.6×10^{-4}
SO_4	1.4×10^{-4}	0.0	bd	2.1×10^{-4}	0.0	bd	1.5×10^{-4}	0.0	bd	1.5×10^{-4}
NO_3	3.7×10^{-5}	0.0	bd	bd	0.0	bd	2.3×10^{-5}	0.0	bd	2.3×10^{-5}
Si	2×10^{-4}	5×10^{-4}	3.5×10^{-4}	7.4×10^{-4}	6.5×10^{-4}	3.6×10^{-4}	7.1×10^{-4}	5.7×10^{-4}	4×10^{-4}	7.1×10^{-4}
NH_4	1.8×10^{-5}	3.7×10^{-4}	2.1×10^{-5}	5.4×10^{-3}	1.4×10^{-5}	7.1×10^{-6}	2.3×10^{-3}	1.3×10^{-4}	5.7×10^{-5}	2.7×10^{-4}
As-tot	1.2×10^{-7}	2.8×10^{-8} (9×10^{-8} Holocene; 2×10^{-7} river muds) [4)]	4.8×10^{-7}	7.9×10^{-6}	3.0×10^{-8}	6.7×10^{-9}	1.0×10^{-7}	9.1×10^{-8}	7.6×10^{-8}	1.0×10^{-7}
Fe	2.3×10^{-6}	1.9×10^{-5}	1.4×10^{-5}	4.9×10^{-4}	2.8×10^{-5}	5.5×10^{-7}	2×10^{-4}	9.6×10^{-5}	4.3×10^{-5}	2×10^{-4}
Mn	7.8×10^{-7}	1.3×10^{-5}	3.0×10^{-6}	4.3×10^{-5}	1.2×10^{-5}	4.1×10^{-6}	5.8×10^{-5}	1.3×10^{-5}	4.1×10^{-6}	1.7×10^{-5}
P	4.2×10^{-7}	1.9×10^{-6} (1.3×10^{-5}) [4)]	3.0×10^{-6}	7.1×10^{-5}	1.4×10^{-6}	8.1×10^{-8}	1.5×10^{-5}	1.0×10^{-5}	5.5×10^{-6}	1.5×10^{-5}
O_2	3.8×10^{-4}	0.0	bd	bd	0.0	bd	8.8×10^{-5}	0.0	bd	bd
DOC	1.6×10^{-4}	-	-	-	-	-	-	-	-	-

1) model input is concentration at VPNS4;
2) Cl model input concentrations are charge balanced;
3) average water composition based on all available observation bores in the Pleistocene sands and gravel deposits, respectively taken as model input;
4) initial concentrations increased to fall in range of observed sorbed fractions of As and P in Holocene and clay/silt deposits, i.e. As initial concentration: 9×10^{-8} mol/L and P initial concentration 1.3×10^{-5} mol/L in the Holocene sands and As of 2×10^{-7} mol/L in river muds

Extended Data Table 3 | Measured and modelled initial concentration of minerals, arsenic solid phase and organic matter. Units are in [mol/L of bulk aquifer volume]. Sorbed initial concentrations are not predefined in the model but the product of initial dissolved concentrations (extended data Table 2) and iron oxide concentration in the sediment (extended data Table 3) (nd = not determined; n/a = not applicable)

	Measured		Data Source	Initial model concentration
	median	range		
Fe(III) oxide	**mg/kg**	**mg/kg**		**mg/kg**
Riverbed	nd [2]	nd [2]	[2]	6200 [2]
Clay/Silt	7472	3640-11304	Eiche (2009) [1]	6200
Holocene Sand	5690	1225-11851	Eiche (2009) [1]	4600
Pleistocene Sand	7943	5001-12630	Eiche (2009) [1]	6200
Gravel	0	0	Eiche (2009) [1]	0
1) Sequential analysis steps F4+F5 = Fe oxide fraction. 2) Riverbed deposits were not analysed as part of the Eiche (2009) study [23], but solid phase concentrations were assumed to be comparable to compositions found in the near-surface clay and silt deposits.				
As total solid phase concentration and leachable fraction	**mg/kg**	**mg/kg**		**Initial sorbed model conc. mg/kg[5]**
Riverbed – total As – total As – leachable As	29 - nd	19 – 50 ≈ 1.5 – 4.4[4]	Stahl et al. (2016) Postma et al. (2010) -	n/a n/a 6.1
Clay/Silt – total As – leachable As (F1 extraction step) – leachable As (F1+F2 extraction step)	11.1 0.2 6.8	5-27.2 0.03 – 2.4 1.8 – 27.2	Eiche (2009) [3] Eiche (2009) [6] Eiche (2009) [6]	n/a 0.1
Holocene/Pleistocene Sand – total As – total As – leachable As (F1 extraction step) – leachable As (F1+F2 extraction step)	 5.8 - 0.03 0.06	 1-30 ≈ 0.4 – 0.6 [9] 0.01 – 1 0.01 – 16.3	 Eiche (2009) [3] Postma et al. (2010) Eiche (2009) [6] Eiche (2009) [6]	 n/a n/a 0.05 – 0.6 [7]
Gravel	nd	nd		0
Organic matter	**wt%**	**wt%**		**Initial model concentration wt%**
Riverbed	nd	nd	[2]	0.1
Clay/Silt	0.08	0.01-0.8	Eiche (2009) [3]	0.05
Holocene/Pleistocene Sand	0.02	0.01-0.1	Eiche (2009) [3]	0.05
Gravel	nd	nd		0
Calcite	**wt%**	**wt%**		**wt%**
Riverbed	nd	nd	[2]	0.8
Clay/Silt	1	0.4-1.8	Eiche (2009) [3]	0- 0.8[8]
Holocene Sand	0.3	0.1-0.7	Eiche (2009) [3]	0- 0.8[8]
Pleistocene Sand	0	0	van Geen et al. (2013)	0
Gravel	nd	nd		0
3) Elemental conc. of bulk sediment (based on X-ray fluorescence analysis). 4) Based on parallel extractions of Red River muds with ascorbic acid forcing reductive dissolution of Fe(III)-minerals. 5) Assuming a bulk density of 1.8 g/cm^3 6) Sequential analysis step F1 and step F1 + step F2. F1 = loosely bound As; F2: strongly adsorbed As. 7) Initial sorbed concentrations in the model fall within a range, due to differences in Fe(III) oxide concentrations (see Table 3) and differences in surface complexation model between Pleistocene and Holocene. 8) Calcite concentration decreasing linearly from Holocene (0.8wt%) to 0 wt% within the Pleistocene 9) Based on parallel extractions of reduced aquifer sediments with ascorbic acid forcing reductive dissolution of Fe(III)-minerals				